CLIMATOLOGY

Past East Asian monsoon evolution controlled by paleogeography, not CO_2

Alex Farnsworth[1,2]*, Daniel J. Lunt[1,2], Stuart A. Robinson[3], Paul J. Valdes[1,2], William H. G. Roberts[4], Peter D. Clift[5,6], Paul Markwick[7], Tao Su[8], Neil Wrobel[9], Fran Bragg[1,2], Sarah-Jane Kelland[9], Richard D. Pancost[2,10]

The East Asian monsoon plays an integral role in human society, yet its geological history and controlling processes are poorly understood. Using a general circulation model and geological data, we explore the drivers controlling the evolution of the monsoon system over the past 150 million years. In contrast to previous work, we find that the monsoon is controlled primarily by changes in paleogeography, with little influence from atmospheric CO_2. We associate increased precipitation since the Late Cretaceous with the gradual uplift of the Himalayan-Tibetan region, transitioning from an ITCZ-dominated monsoon to a sea breeze–dominated monsoon. The rising region acted as a mechanical barrier to cold and dry continental air advecting into the region, leading to increasing influence of moist air from the Indian Ocean/South China Sea. We show that, apart from a dry period in the middle Cretaceous, a monsoon system has existed in East Asia since at least the Early Cretaceous.

INTRODUCTION

The East Asian monsoon (EAM) system plays a fundamental role in the transport of energy from the tropics to the extra tropics. The sensitivity of the EAM to changing future greenhouse gas concentrations has been the subject of intense research focus [(*1*) and references therein] because the EAM influences the lives of more than a billion people. As the monsoon changes, it may alter the risk of drought or flooding (*2*) and necessitate changes to the large-scale agriculture that is needed to sustain the population. Despite recent progress, considerable uncertainty remains even as to the sign of change of EAM precipitation in a warmer world (*1*).

Climates in the geologic past that were characterized by high atmospheric carbon dioxide concentrations (pCO_2) (*3*) and temperatures that were warmer than today allow the behavior of key climatic processes, including monsoon systems, to be investigated. It is now well established that East Asia (EA) in the Early Neogene [23 to 16 million years (Ma)] was monsoonal (*4*–*6*) [where a monsoon is defined throughout this paper as >55% of annual precipitation falling during local summer (May–September) and local summer-minus-winter precipitation rate being >2 mm/day (*7*)], and it has recently been suggested that the Late Eocene (~40 Ma) was characterized by a monsoonal climate (*8*, *9*); both are periods when global temperature was substantially higher than modern (*10*), challenging the Neogene onset hypothesis. However, the detailed evolution of past monsoonal changes is uncertain, and the underlying causes are poorly understood. Furthermore, investigation of the sensitivity of the EAM to paleogeography and CO_2 has only focused on the modern or single past time slices, rather than exploring secular changes.

[1]School of Geographical Sciences, University of Bristol, Bristol BS8 1SS, UK. [2]Cabot Institute, University of Bristol, Bristol BS8 1UJ, UK. [3]Department of Earth Sciences, University of Oxford, Oxford OX1 3AN, UK. [4]Department of Geography and Environmental Science, Northumbria University, Newcastle upon Tyne, UK. [5]Department of Geology and Geophysics, Louisiana State University, Baton Rouge, LA 70803, USA. [6]Research Center for Earth System Science, Yunnan University, Chenggong District, Kunming, Yunnan 650091, PR China. [7]Knowing Earth Limited, Otley, West Yorkshire, UK. [8]CAS Key Laboratory of Tropical Forest Ecology, Xishuangbanna Tropical Botanical Garden, Chinese Academy of Sciences, Mengla 666303, China. [9]Getech Group plc, Leeds LS8 2LJ, UK. [10]Organic Geochemistry Unit, School of Earth Sciences, and School of Chemistry, University of Bristol, Bristol BS8 1RJ, UK.
*Corresponding author. Email: alex.farnsworth@bristol.ac.uk

Both paleogeography (*4*, *5*, *11*, *12*) and changes in p_{CO_2} (*1*, *8*, *12*–*17*) have been proposed as key drivers of EAM past, present, and future evolution; however, there is also uncertainty as to the role of CO_2, with some studies suggesting that increasing CO_2 will not have an impact on the future EAM (*18*–*21*). Other future warming projections suggest an increase in intensity in the EAM (*1*, *14*), but many uncertainties remain, with the modern observational record suggesting no clear trends during the 20th century (*14*).

Changing paleogeography has had a major influence on the climate system, especially the hydrologic system (*22*, *23*), by perturbing past atmospheric and oceanic circulation and energy fluxes. An important paleogeographic feature that may have contributed to a change in the monsoon is the uplift of the Himalayan-Tibetan region (HTR) (*4*, *5*, *11*). Although the evolving geometry of the HTR is widely debated (*24*, *25*), the continental collision between India and Eurasia is thought to have commenced in the Early Eocene, ~50 Ma (*26*), and likely no later than 40 Ma (*27*). Other paleogeographic features that may have an influence on EAM development include the Tethys Ocean (*28*) and the Iranian plateau (IP) (*29*). pCO_2 affects monsoons by modifying thermal gradients, atmospheric heating, and water vapor content, which all can have nonlinear impacts on precipitation. pCO_2 changes over geological time are uncertain (*3*), although multiple proxies indicate that values were relatively high during much of the Cretaceous, Paleocene, and Late Eocene (~145 to ~40 Ma) and have declined since that time (Fig. 1C) (*3*, *30*). Here, we assess the relative importance of these two key proposed drivers for the origins and intensity of the EAM.

Quantifying the geologic long-term monsoon evolution, excluding short-term transient events such as the Paleocene-Eocene Thermal Maximum, is problematic because of the temporal and spatial sparsity of proxy records and uncertainties in their interpretation. Paleoclimate modeling can provide important insights by simulating monsoon evolution in response to prescribed changes in environmental drivers and by carrying out model-data comparison with the available data.

Previous attempts to understand the mechanisms behind EAM evolution have focused on specific time periods (*8*, *11*–*13*) and often used a limited range of proxies over a localized area. While some studies (*8*, *12*) have attempted to disentangle the impact of perturbing pCO_2 and paleogeography on monsoons for singular time slices, no attempt has been made to quantify their relative roles through geologic time.

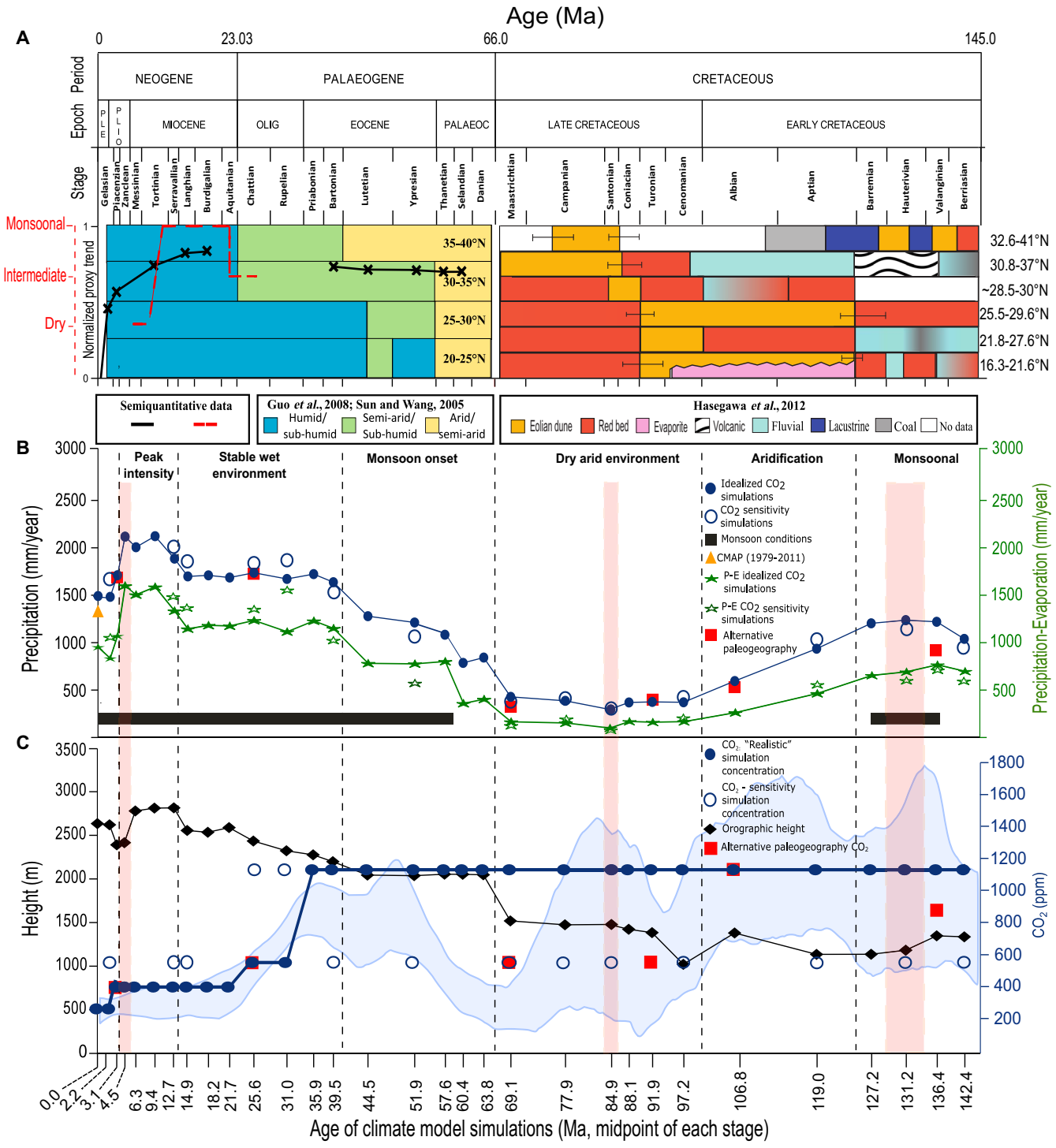

Fig. 1. Data-model precipitation, pCO_2, and HTR trend through time. (**A**) Normalized quantitative precipitation proxy data trend (solid black line) is shown in conjunction with two qualitative proxy data compilations for the Cretaceous (*31*) and for the Paleogene and Neogene (*4*, *6*) within 16°N to 41°N, 75°E to 130°E. Both colored panels in (A) are independent of either of the left *y* axis and indicate the intensity of the hydrologic cycle. The dashed red line (*32*) is a compilation of proxies from ocean drilling program sites 1146 and 1148 indicating monsoonal conditions. See the Supplementary Materials for details. (**B**) EA modeled mean annual precipitation (mm) for each geologic stage (region: fig. S4) at idealized CO_2 (closed blue circle), sensitivity CO_2 (open blue circle) concentrations, and alternative paleogeography (red square). The mean annual precipitation minus evaporation (mm) for each geologic stage at idealized CO_2 (closed green star) and sensitivity CO_2 (open green star) concentrations is shown. Black horizontal bar represents model-derived monsoonal conditions present. Orange triangle represents the mean annual (1979–2011) precipitation for the monsoon region from CMAP observations. (**C**) Mean orographic height (m) between 27.5°N and 45°N, 71.25°E and 101.25°E for each geologic stage (diamonds) and CO_2 concentrations (circle/square) for each simulation. Shaded blue band signifies range in proxy CO_2 uncertainty (*3*). Red vertical boxes (B and C) represent the three synthesized key periods investigated in this study. PALEAOC, Paleocene epoch; OLIG, Oligocene epoch; and PLE, Pleistocene epoch.

Here, we take a more complete approach, exploring the evolution of the EAM throughout the past 145 Ma using a suite of high temporal resolution snapshot climate model simulations to understand the interplay between different forcing mechanisms during different time periods. We present a synthesis of existing paleohydrological proxies over the duration covering the regional scale where available, compare this with the series of new model simulations, and investigate the drivers and mechanisms influencing EAM evolution.

RESULTS

Geological evidence of EA hydrology evolution

We first analyze multiple different proxies within the EAM region, taking account of plate tectonic movements (fig. S4) through a synthesis and reanalysis of existing qualitative and quantitative proxy data records of EA hydrological cycle evolution. The use of multiple proxies can reduce uncertainty because (i) a single site cannot record the spatial extent of the monsoon or distinguish between a change in the movement of the monsoon from that of an overall change in intensity, and (ii) multiple proxies reporting the same trends make for a more robust signal. The qualitative data record (Fig. 1A, horizontal bars and red dashed lines) is based on previous sedimentological studies (*4*, *31*–*34*). The quantitative data record (Fig. 1A, black solid lines) is calculated from precipitation estimates (table S1) derived from the fossil record, averaged over the sites available for each geological stage in our defined EAM region.

Qualitative proxies of Cretaceous climates (Fig. 1A) (*31*) generally indicate humid conditions in EA during the earliest Cretaceous (evidenced by coal-bearing sediments and lacustrine and fluvial deposits), drying through the mid-Cretaceous, with relatively humid conditions ceasing by the earliest Late Cretaceous (~100 Ma; as indicated by arid and semiarid conditions suggested by evaporites, aeolian dunes, and red beds bearing calcretes). Dry conditions persist in the record until the end of the Cretaceous. Similar quantitative and qualitative paleobotanical and lithological proxies (Fig. 1A) (*4*, *6*) suggest that the environment became more humid through the Paleocene, Eocene, and Oligocene to the Miocene (signified by a shift from evaporitic deposits and pollen indicative of arid conditions such as *Ephedripites* to mudstones and pollen produced by more moisture-demanding taxa such as *Taxodiaceaepollenites*). Other qualitative evidence (Fig. 1A, red dashed lines) (*5*) indicates that the local hydrological cycle intensity peaked in the Early to Middle Miocene (~20 Ma) and then declined during the Late Miocene and Pliocene.

Quantitative proxies (Fig. 1A, black lines) (*34*–*36*) are lacking for EA in the Cretaceous but show a relatively stable hydrological cycle through the Late Paleocene and Eocene. Following a hiatus in the Oligocene, there is evidence for a maximum hydrological intensity in the Early Miocene, decreasing toward the preindustrial.

Modeled evolution of the EA monsoon

Using the HadCM3L coupled atmosphere-ocean climate model (see the "Model simulations of monsoon evolution" section in the Supplementary Materials), we carry out a set of 38 simulations covering the Cretaceous to the preindustrial, one for each stratigraphic stage, with varying paleogeography, pCO_2, and solar constant. The prescribed paleogeographies (fig. S1) are consistent with paleoaltimetry data (table S3 and fig. S2; see the "Qualitative records" section in the Supplementary Materials). Atmospheric CO_2 concentrations in the model are held constant [1120 parts per million by volume (ppmv)] through the Cretaceous, Paleocene, and Eocene and then decrease through the remainder of the Cenozoic, toward preindustrial values of 280 ppmv (Fig. 1C, closed circles), as very broadly indicated by CO_2 proxies (*3*). In addition, for 14 stages, we carry out sensitivity tests with different CO_2 concentrations (Fig. 1C, open circles). Furthermore, for six stages, we carry out additional simulations with alternative paleogeographic reconstructions (Fig. 1C, red squares; see the Supplementary Materials). Initially, we evaluate the modeled preindustrial monsoon region (fig. S4) against observed data, which demonstrates that our model can simulate the broad-scale features of the monsoon system sufficiently well (see the "Model simulations of monsoon evolution" section in the Supplementary Materials). This finding is also supported by Dabang *et al.* (*37*) and Sperber *et al.* (*38*) who showed that HadCM3 simulates the climate of the monsoon region better than other contemporary models (*38*).

Modeled precipitation is relatively stable in the first 30 Ma of the Cretaceous (Berriasian to Barremian; Fig. 1B), with regional annual mean monsoonal precipitation of ~1300 mm/year (Fig. 1B, orange triangle) [similar to observed modern values (*39*)]. Seasonal precipitation [supported by proxy evidence (*40*)] has a unimodal distribution, similar to that of the modern (fig. S3). Furthermore, the modeled precipitation-evaporation, which may better represent the controls on the various proxy records, shows similar trends to those of the precipitation (this comment applies for all modeled time periods; Fig. 1B). A clear wet-dry-wet-dry latitudinally banded precipitation signal is also simulated, which shows good agreement with geologic and phytogeographical evidence (Fig. 1A) (*31*).

In the latter part of the Early Cretaceous, modeled precipitation decreased (and is no longer monsoonal). By the Late Cretaceous, EA had become arid (Fig. 1B), and this dry climate dominated the region except for Pacific coastal areas. There is an increase in precipitation from the end of the Cretaceous to the end of the Eocene when values are again similar to the preindustrial. Reemergence of the simulated monsoon occurs during the Paleocene (fig. S4). A reduction in the length of the monsoon season is simulated for the Paleocene in southern EA, with most of the Eocene showing weakened monsoonal conditions (fig. S3), in agreement with seasonal proxies (*9*). Precipitation remained constant from the mid-Late Eocene until the Early Miocene at values exceeding 1700 mm/year. A shift in seasonality is simulated during the Paleocene-Oligocene together with an extended monsoon season (Priabonian-Chattian; 37.8 to 23.0 Ma).

From the Middle Miocene (~13 Ma), a distinct increase in annual precipitation is simulated. A period (~4 to ~12 Ma) of "super monsoon" is established. (We use a simple measure, in which a super monsoon is when the annual mean precipitation is $>P + P2\sigma$, where P is the preindustrial 30-year mean of precipitation and $P2\sigma$ is two standard deviations of the interannual variability of the preindustrial precipitation.) Last, there is a decrease in precipitation from the Piacenzian (3.6 to 2.6 Ma) to the preindustrial. During the Neogene (23 Ma to Modern), there is considerable variability in the distribution of seasonal, peak month (May–August), and monsoon onset precipitation (March–May). During the Miocene, the wet season is modeled to be more persistent through the year (an extension of the monsoon season earlier in the year by 1 to 2 months; fig. S3).

Although comparison of the various qualitative and quantitative proxy records with the modeled precipitation and precipitation minus evaporation (P − E) results is challenging, there is broad agreement between them with respect to the general trends. The proxies and model indicate a drying through the Cretaceous, followed by increasing precipitation through the Paleogene, a precipitation peak in the Middle

Miocene, and then drying toward the preindustrial. In addition to the proxy data used to characterize trends, we also compile proxy data from additional sites where precipitation data exist only for a single stratigraphic stage (table S1), with model data showing generally a good fit to the proxy data.

Drivers of monsoon evolution: Paleogeography versus pCO_2

First, we assess the relative role of paleogeography versus pCO_2 in determining the monsoon evolution. To this end, we carried out 14 sensitivity studies in which pCO_2 was prescribed as half or double the default values (Fig. 1, B and C, open circles). This shows that the pCO_2 concentration has a much weaker control on monsoon evolution than paleogeography (Fig. 1, B and C). In the sensitivity studies, a pCO_2 doubling only marginally affects EAM precipitation (−1 to +13%; Fig. 1B), which is a small effect compared with changes in paleogeography. In particular, the subsidiary role for pCO_2 in comparison to paleogeography is highlighted by the constant modeled monsoon intensity from the Eocene to the Oligocene, a period when the prescribed pCO_2 markedly declines at the Eocene (1120 ppm)–Oligocene (560 ppm) transition. The robustness of our results to the paleogeographic reconstruction is illustrated by our simulations with alternative paleogeographies (Fig. 1B, red squares). These alternative simulations indicate a similar trend to our standard simulations, showing that the modeled precipitation is not generally sensitive to the details of the paleogeographic reconstruction. However, the small differences in the regional topography may have an impact on the precipitation signal in the Valanginian (Fig. 1B; contrast paleogeographies in fig. S1xxix with fig. S10).

Paleogeographic control on monsoon evolution

Over the past ~150 Ma, there have been changes to numerous paleogeographic features that could be responsible for the modeled monsoon evolution. Isolating these regional features, the associated mechanisms, and the interplay between them would require many hundreds of model sensitivity studies, beyond the computational resource of this study. However, by examining the modeled response over time, we can suggest plausible mechanisms that are consistent with the broadest features of the modeled EA precipitation over this period (Fig. 1B).

The decreasing trend in precipitation from the mid-Early Cretaceous to the Late Cretaceous, during which pCO_2 was held constant in our simulations, can be attributed to a number of phenomena related to paleogeography. First, the progressive decrease in continental area between 30°N and 50°N and the increase between 70°N and 80°N changes the latitudinal gradient of continental area to create a decrease in the summer temperature gradient between the mid- and high latitudes (fig. S5B). This is associated with a weakening and equatorward shift in the Hadley circulation (Fig. 2, A and B, and table S3). Second, convective (parameterized) processes are increasingly inhibited by a mid-tropospheric anticyclone centered at ~30°N, 90°E (Fig. 2, A and B), which is likely a response to early surface uplift in the region (see Fig. 1C). This anticyclone, whose formation and location are associated with large-scale thermal forcing (*41*), inhibits the EAM by capping organized moisture penetration below 500 hPa, advecting dry continental northwest (NW) air into the EAM region. There is a progressive strengthening of this anticyclone through the Cretaceous; it reaches its strongest in the Santonian (~84 Ma), the driest period during the EAM evolution (Fig. 1. A and B). Third, there is a shift in the Pacific warm pool from the West Pacific toward the mid-Pacific with an associated decrease in moisture transport in the EAM region via the Walker circulation.

During the Late Paleocene, the EAM reemerged and progressively strengthened through the Cenozoic based on the amount of seasonal precipitation (June–September) and its seasonal range (table S3). This is associated with the Pacific warm pool migrating back toward Asia, and the continuing topographic evolution of the HTR caused by the collision of the Indian and Asian continental plates. A proto-Siberian High is present through most of the year, with modeled central Asian surface circulation in agreement with paleo-wind reconstructions (*42*). The strengthening of the monsoon coincides with the maximum extent of the Hadley circulation migrating poleward from near the equator at the end-Cretaceous to 20°N in the Paleocene and 30°N in the late Eocene. From the Eocene to the middle Miocene, the monsoon continued to strengthen and expand. During the Eocene, a weak "sea-breeze" monsoon circulation, similar to, but much weaker than, that which dominates EA today, is present in the simulations (Fig. 3). The strength of this sea-breeze circulation increases through the Eocene to the Pliocene and then decreases toward the preindustrial. These results suggest that, during the Eocene, the monsoon was dominated by the seasonal latitudinal migration and strengthening of the Hadley circulation [i.e., an intertropical convergence zone (ITCZ)–type monsoon], also suggested by proxy evidence (*43*), rather than a sea-breeze circulation (Fig. 3 and table S3). Nonetheless, by the Miocene, the sea-breeze circulation dominates, driven by strengthening thermal gradients associated with evolving paleogeography.

The modeled onset of monsoon conditions and increasing precipitation during the Paleocene is synchronous with an uplift in orography in the region of the HTR, and the maximum intensity of the monsoon in the Miocene coincides with the maximum in HTR topography, following break-off of the subducting Indian lithosphere (*44*). From the Danian (~63 Ma), there is a progressive weakening and westward propagation of the thermal low and associated anticyclone, toward the western portion of the HTR away from the EAM region, no longer being an inhibitor to large-scale precipitation formation. In the model topography, once the HTR region reaches a mean height of between 2300 and 2400 m, the anticyclone is lifted further into the troposphere to ~200 hPa. The relationship between the mean HTR topographic height and modeled precipitation is supported by a strong positive correlation ($r^2 = 0.87$) from the mid-Cretaceous to the preindustrial (Fig. 1C, black line). This strongly highlights the importance of topographic height and breadth in strengthening monsoon systems in EA. Outside of the EAM region, persistent dry central Asian conditions over the past 42 Ma suggest that the evolution of the Paratethys Sea may have had little impact on atmospheric circulation, consistent with the proxy data reconstructions by Licht *et al.* (*42*), suggesting that the large-scale model atmospheric circulation is consistent with proxy observations.

The decrease in precipitation from the Pliocene is likely associated with the decrease in the height of the Iranian Plateau (IP) (fig. S1, i to iii) due to a reduction in near-surface southerlies and vertical advection of tropical air masses whose transport pathway is aided by a high IP into the EAM region. This suggests that there is a reduction in circulation coupling between the tropics to subtropics and the mid- to upper troposphere. This reduces the flux of moisture to higher latitudes and results in a southerly shift in the rainbelt in EA. Wu *et al.* (*29*) also see a similar response in a more idealized study in which the IP was removed. The Meiyu-Baiu front also weakens in response to a weakened low-level jet on the equatorward side of the front. Advection of moisture from the South China Sea/Indian Ocean and northward monsoon flow weakens

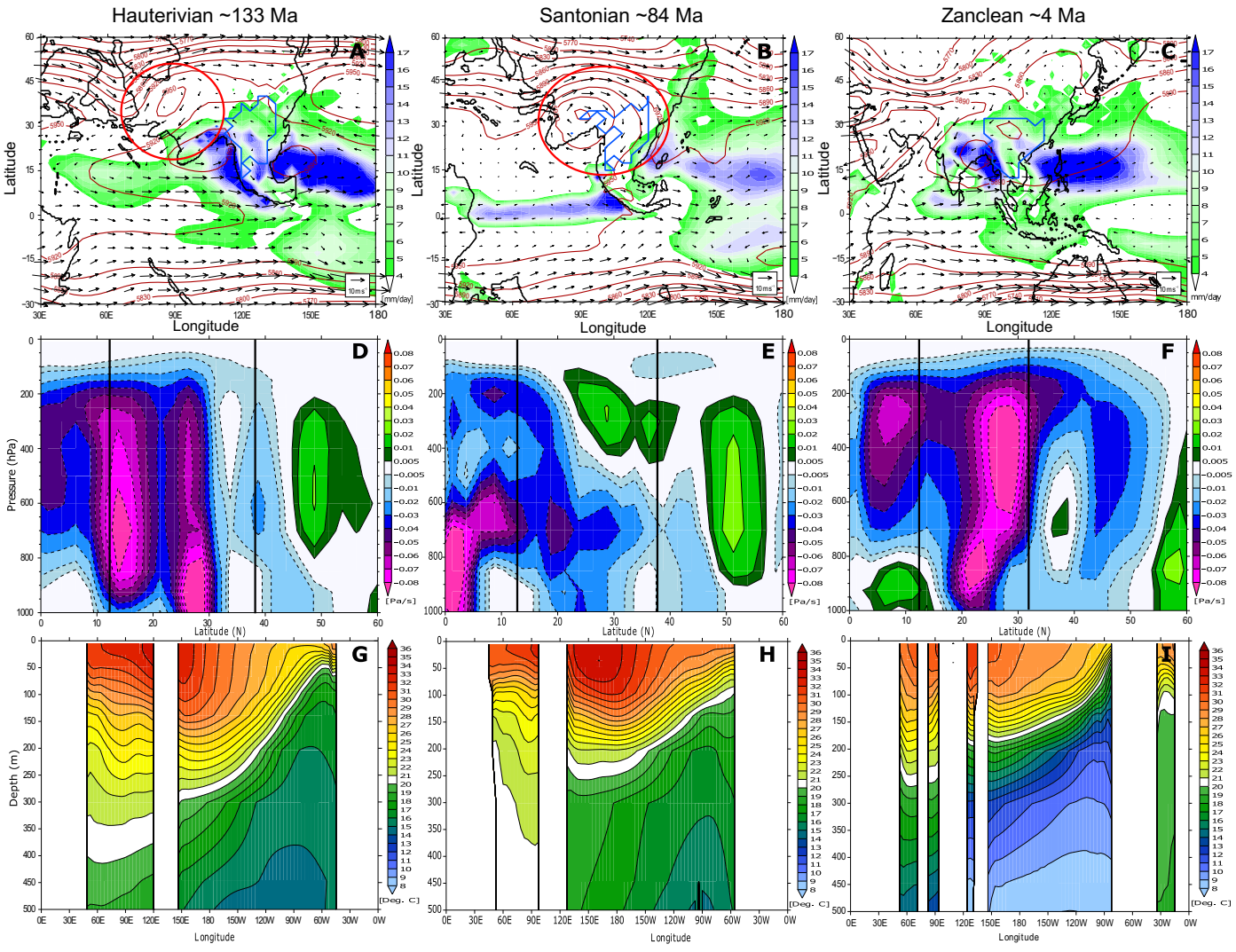

Fig. 2. Atmosphere-ocean dynamics of three key periods. Wettest month 500-mbar geopotential height (isolines), wind field (black arrows), and precipitation in the Hauterivian (**A**), Santonian (**B**), and Zanclean (**C**) (paleo-rotated region in blue line). Wettest month zonal cross-sectional (0°N to 60°N, 105°E to 112.5°E) vertical velocity in the Hauterivian (**D**), Santonian (**E**), and Zanclean (**F**) depicting the position of the Hadley circulation; negative values indicate vertical ascent, positive values indicate vertical descent, and vertical black lines depict maximum and minimum latitudinal extent of rotated EAM region. Mean annual meridional (10°S to 10°N) depth profile ocean temperature (°C) for the Hauterivian (**G**), Santonian (**H**), and Zanclean (**I**) depicting the location of the Pacific warm pool. Red circles denote region of interest highlighted in the main text.

from a reduction in the coupling strength between the tropics and the subtropics associated to a decrease in the IP height.

In summary, we suggest that the decrease in precipitation from the Early Cretaceous to Late Cretaceous is due to a combination of changes in gradient in continental area and local uplift, the pole-to-equator thermal gradient, and the location of the Pacific warm pool. The increase in precipitation toward the super monsoon of the Middle Miocene is caused by uplift of the HTR, and the decrease from the Pliocene toward the preindustrial is caused by the decrease in height of the IP.

Paleogeographic dynamical controls on monsoon evolution

Here, we concentrate on three key intervals over the past 145 Ma and focus on the influence of paleogeographic forcing and the dynamical mechanisms that it invokes.

i) Early Cretaceous monsoon

The Hauterivian (~131 Ma) is characteristic of the dynamics of the Early Cretaceous monsoon period (conceptualized in Fig. 4A). The model simulates annual precipitation of ~1250 mm/year in the EAM region. The seasonal maximum in precipitation lasts from July to September (compared with June–September in the Modern; fig. S3). The EAM is likely dominated by the northerly branch (~10°N to 20°N 120°E) of the main westerly flow into the EA region at 850 hPa (Fig. 4A and fig. S7G, green circle), which is similar in structure to the preindustrial Somali low-level jet (SLLJ). In addition, a southern arm of the SLLJ circles back through the South China Sea and into EA from the east, entraining additional moisture (Fig. 4A and fig. S7G, red circle). Furthermore, the ascending branch of the Hadley circulation is centered directly over the south EAM region in the Hauterivian (Fig. 2D). Convective processes are enhanced by stable outflow (10°N to 25°N) high in the

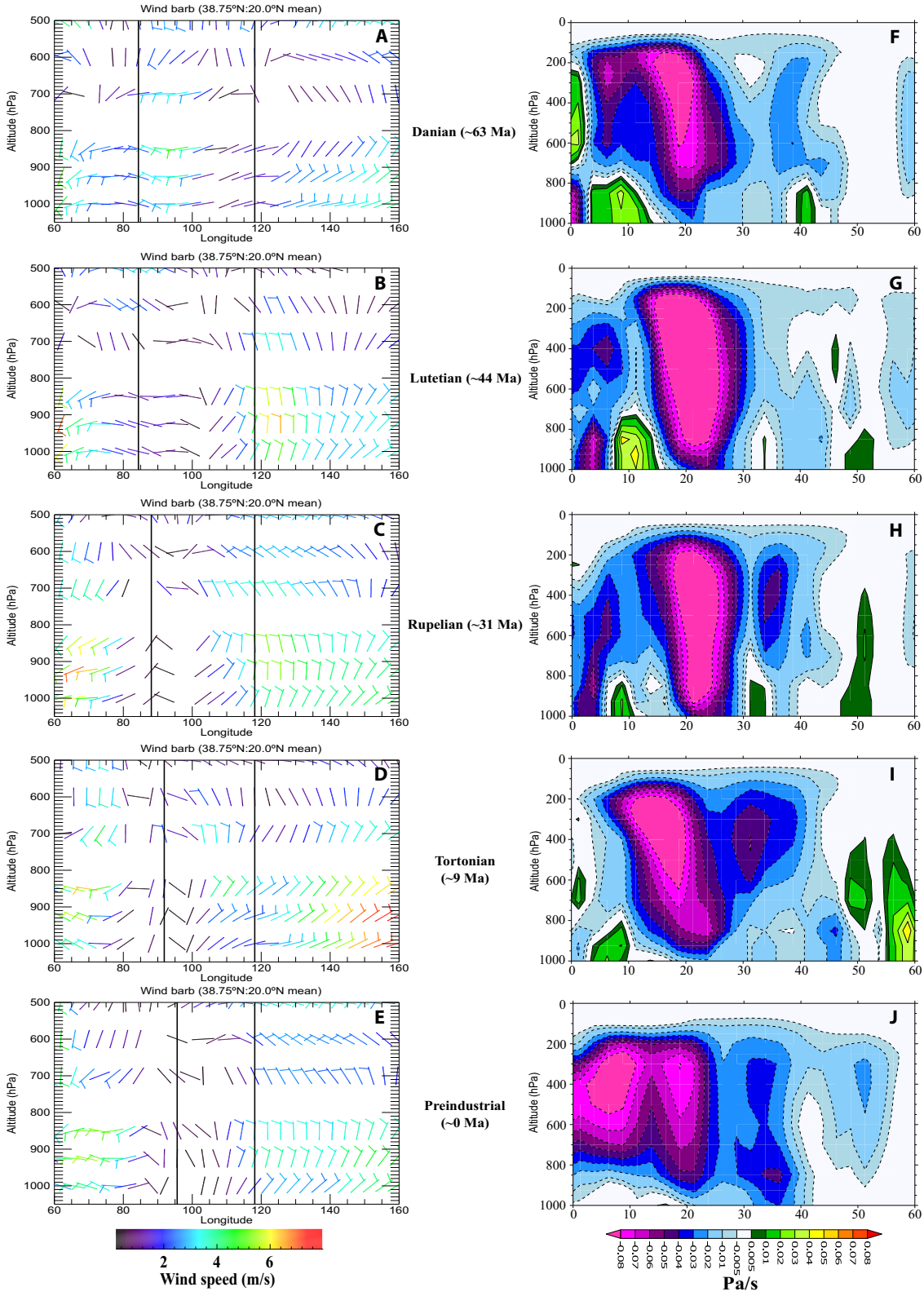

Fig. 3. EA summer (June–August) sea-breeze and maximum Hadley circulation extent. Zonal (June–August) sea-breeze circulation (left-hand column) indicated by wind barbs showing direction and magnitude (m/s; color scale) for the Danian (**A**), Lutetian (**B**), Rupelian (**C**), Tortonian (**D**), and preindustrial (**E**). Vertical black lines depict the maximum and minimum longitudinal extent of the EAM region (mean, 38.75°N to 20°N). Meridional vertical velocity (Pa/s; right-hand column) cross section (mean, 105°E to 112.5°E) in the EAM region showing the maximum northerly extent of the Hadley circulation in the boreal summer. Negative values indicate vertical ascent, while positive values indicate vertical descent for the Danian (**F**), Lutetian (**G**), Rupelian (**H**), Tortonian (**I**), and the preindustrial (**J**).

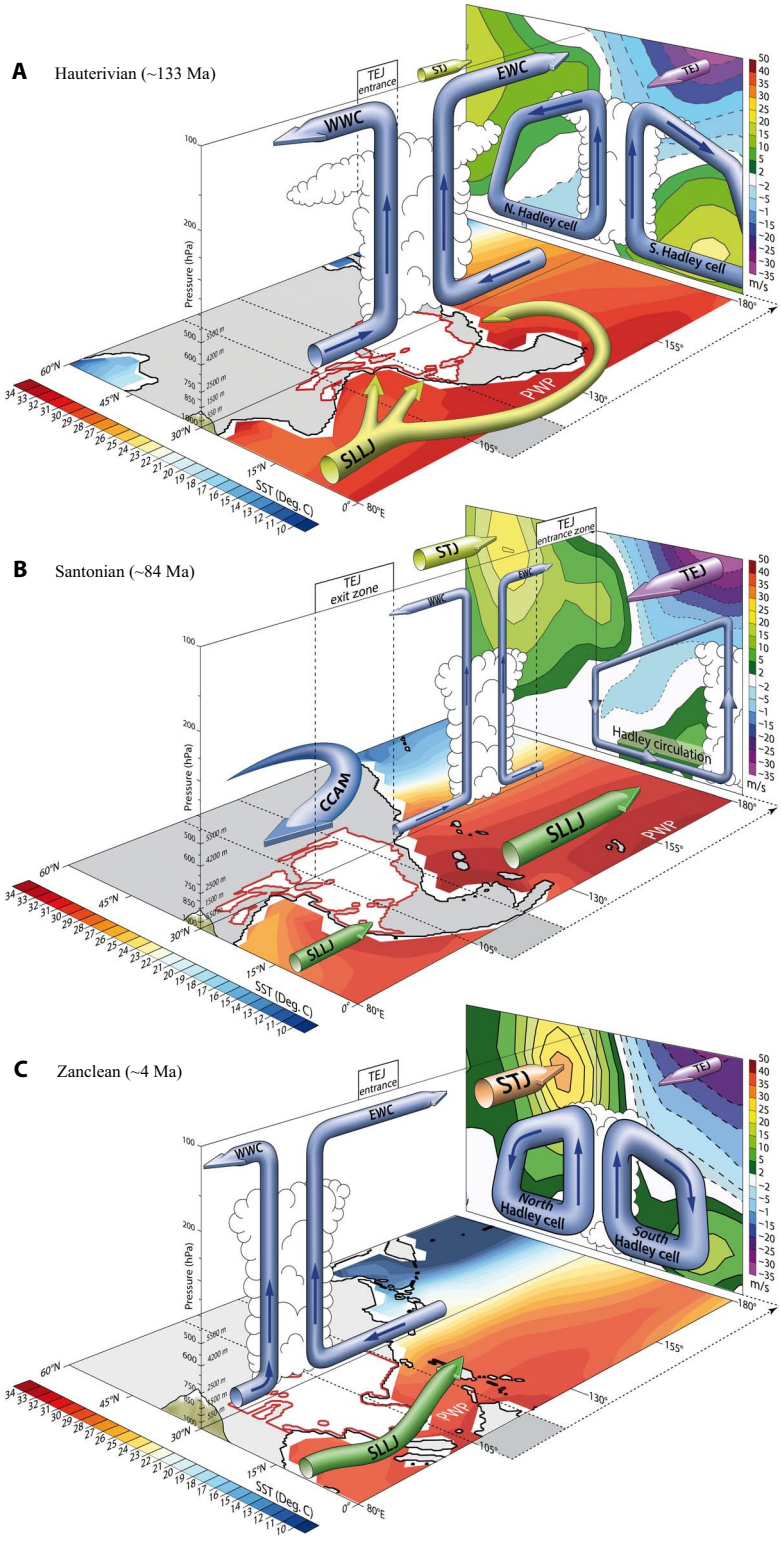

Fig. 4. Conceptualized model of each key period. Schematic of the key processes leading to the weak monsoon in the Hauterivian (**A**), dry period of the Santonian (**B**), and super monsoonal conditions in the Zanclean (**C**) in the EAM region depicting a collation and synergy of model data. The wettest month of the monsoon season sea surface temperatures (SSTs) (°C) and zonal wind cross section (m/s; mean, 105°E to 112.5°E) is depicted. Arrow thickness represents the intensity of the process. Blue arrows indicate advection of air masses. WWC, western Walker cell; EWC, eastern Walker cell; STJ, subtropical jet; TEJ, tropical easterly jet with both its entrance and exit zone shown. The white "cloud" represents the region of deep organized convection, where the atmospheric dynamics highlighted in these schematic produces conditions for intense rainfall. PWP indicates the position of the Pacific warm pool. The white landmass with red outline represents the paleo-rotated location of EAM. The vertical axis on the left-hand indicates both atmospheric pressure (hPa) and height (m). The height of the HTR is also indicated on the cross section between the left-hand *y* axis and latitudinal *x* axis.

atmosphere (200 hPa), present in the south/southwest of the EA region. This stable outflow is itself enhanced by an apparent tropical easterly jet (TEJ) that further ventilates the system (fig. S7J, green circle). The entrance zone of the TEJ is found to the south of the region (fig. S7J, red circle)—this promotes surface convergence to the north of the entrance zone (*45*) in the EAM region.

ii) Late Cretaceous arid period

The Santonian EA climate (conceptualized in Fig. 4B) is simulated as a very dry environment with precipitation of ~310 mm/year, a ~75% reduction compared to modern observations. Seasonal precipitation peaks during June–September (fig. S3). Only a weak proto-SLLJ is formed to the west of the region (Fig. 4B and fig. S7H, green circle). However, a strong cross-equatorial flow [here called the low-level Pacific jet (LLPJ)] crosses the equator at 120°E (fig. S7H, red circle), forming strong westerly flow away from EA. The weakened SLLJ, which features in all simulations of the arid Late Cretaceous (fig. S8), substantially reduces the supply of moisture into the region. The modeled EA surface circulation is in agreement with paleocurrent reconstructions (*46*), with westerlies dominating and weak penetration of onshore flow from the South China Sea (fig. S7H).

The ascending branch of the Hadley circulation (Fig. 2E) is nearer the equator and substantially weaker than during both the Hauterivian and the preindustrial in the model (fig. S6D). Vertical velocities over the region show shallow convection capped to the mid-troposphere (500 hPa; Fig. 2E). The ascending branches of the West Pacific Walker circulation are weaker (defined as the strength in vertical velocities during the wettest month in the monsoon season in the ascending branch of the Walker circulation) and shallower than the preindustrial with convection again capped at 500 hPa (fig. S7E, white circle). The Walker circulation (fig. S7E) is also located further eastward compared to the Hauterivian and the preindustrial, with moist convection suppressed in the EAM region and over the proto–Indian Ocean (fig. S7E, red circle), further reducing moisture transport into EA. This eastward shift of the ascending branch of the Walker circulation (fig. S7F, white circle) away from the EAM region is in response to an eastward shift in the Pacific warm pool to the mid-Pacific (Fig. 2H), and a similar atmospheric reorganization is seen under observed modern El Niño–Modoki conditions, which also weakens the EAM (*47*). The shift in the warm pool is a result of the weakening of the northeasterly (NE) trade winds, which is a response to the weakened Hadley circulation and the opening of the Western Interior Seaway (WIS), an open oceanic gateway between the western interior of the North American continental plate between the Arctic Ocean and Caribbean Sea through the mid-Late Cretaceous. An open WIS in the model has a marked impact on the atmospheric and oceanic circulation of the Pacific. With an open WIS, the boreal summer diabatic heating rates over the seaway and western American continent are weakened. This reduced heating weakens the western Pacific subtropical high (*48*). This is a robust feature of many climate models (*49*). A weaker subtropical high diminishes equatorward flow, which further weakens the NE trade wind and the incursion of northerlies down the EA coastline. These cold and dry winds inhibit the advection of moist air masses from the South China Sea and only allow shallow convection to occur, reducing precipitation in EA. Further, a slackening of the NE trade winds is likely leading to shift in this warm pool to the mid-Pacific and El Niño–Modoki conditions.

In addition, dry continental NW winds in the mid-troposphere (Fig. 2B, red circle) driven by thermal forcing from elevated topography further suppress deep convection over inland EA. A stronger and more southerly extending subtropical jet (fig. S7B, red circle), a consistent feature throughout the Late Cretaceous, also inhibits the northerly extent of the monsoon system. The TEJ entrance zone (mid-Pacific) is east of the EAM region, potentially linked to the eastward propagation of the Pacific warm pool, with the exit zone over the south of the region (fig. S7K, red circle). This causes surface divergence in regions north of this exit zone, further inhibiting convection. These combinations of factors lead to the suppression of the EAM during the Cretaceous.

iii) Middle Miocene/Pliocene "super-monsoons"

The Zanclean (~5.3–3.6 Ma; conceptualized in Fig. 4C) during the Pliocene represents the strongest simulated EAM, with precipitation of ~2100 mm/year, a ~30% increase compared to preindustrial levels. Seasonal precipitation is unimodal, with an earlier monsoon season (May–August) than the preindustrial, and high precipitation simulated in April and September, which suggests an extended monsoon period.

The SLLJ intensifies during the Neogene (fig. S8) and is near its maximum strength in the Zanclean (~13 m/s compared with 3 m/s in the Middle Cretaceous). The intensified SLLJ is a dominant feature allowing greater moisture flux into the south and west of EA (fig. S7i, green circle). An intensified ascending branch (Fig. 2F) of the Hadley circulation, compared to the Hauterivian, Santonian, and preindustrial (Fig. 2, D and E, and fig. S6D, respectively), is prominent between 15°N and 35°N (with convection enhanced up to 50°N), increasing precipitation recycling in regions far from the original moisture source. The latitudinal position (10°N to 20°N) of the SLLJ (fig. S7I, green circle) and the location of the ascending branch of the Hadley circulation provide conditions for the penetration of sustained mesoscale convective systems into the usually dry interior of mid-NW China (Fig. 2C). Precipitation is further enhanced by the ascending branches of the east and west Walker cells within the longitudinal boundaries of EAM region (fig. S7F).

An intensified subtropical jet (Zanclean, ~30 m/s; preindustrial, ~15 m/s; fig. S6E for comparison) and weak Polar jet configuration (fig. S7C, red and white circle, respectively) in the Zanclean simulation aids the intensification of a Meiyu-Baiu front feature (*50*), a quasi-persistent, near-stationary, east-west (from Japan to Tibet) orientated zone of weak baroclinity. This is a persistent quasi-stationary front associated with high precipitation from convective complexes propagating eastward along this front formed from the confluence of warm moist monsoonal and cold northerly air mass system in modern observations (*51*).

DISCUSSION

We show that changes in paleogeography are primarily responsible for the evolution of the EAM over the last ~145 Ma and that CO_2 has little control on the EAM intensity.

We demonstrate that during the Early Cretaceous, monsoonal conditions were present in the EAM region, albeit weaker than the preindustrial corroborated by qualitative proxy data (Fig. 1). The monsoon circulation during this period is different to that of the preindustrial, with low-level advection of moisture from the proto–Bay of Bengal and paleo–South China Sea combined with an intensified Hadley-Walker circulation over the region. This is controlled by a strong pole-equator temperature gradient (fig. S5B), which weakened into the Late Cretaceous due to an increase (decrease) in land surface in higher (mid-) latitudes (tables S3 and S4).

During the Late Cretaceous, a reorganization of large-scale circulation, associated with an eastern migration of the Pacific warm pool (a result of weakened northeast trade winds; Fig. 2), reduced moisture supply to the region and shifted the Hadley circulation equatorward

and the Walker circulation eastward away from EA (fig. S7). This arid environment, consistent with geological data (Fig. 1A), is enhanced by incursion of cold, dry NW continental air mass in the mid-troposphere, which further weakened organized deep convection. This incursion is possible because of a westward migration of the Asian continent toward the center of the anticyclone (fig. S2) and a weakened Western Pacific subtropical high. Previous modeling work has suggested that the Late Cretaceous had a monsoon system similar to the Modern (*16*). However, those findings are inconsistent with our proxy reconstruction of the EAM (Fig. 1A).

EAM precipitation is strongly correlated (table S4) with the intensity/location of the Hadley circulation during the Cretaceous ($r^2 = -0.72$) and the Paleogene ($r^2 = -0.91$), which, in turn, is strongly correlated with the latitudinal temperature gradient ($r^2 = 0.84$ and $r^2 = 0.79$, respectively). In the Neogene, perturbations in the Hadley circulation have little influence on precipitation; instead, a weakening of the Walker circulation (tables S3 and 4) associated with a shoaling of the eastern Pacific thermocline and strengthening of easterlies is coincident with EAM precipitation increase.

During the Neogene, the regional circulation transitioned from an ITCZ-dominated monsoon and started to develop into its preindustrial configuration as a response to the uplift of the HTR, as the incursion of dry NW continental air mass (Fig. 2) reduced and eventually ceased by the Early-Middle Miocene. The dominant control on the EAM is again shown to be paleogeography and not pCO_2 (Fig. 1B), in contradiction to Licht *et al.* (*8*). Trends in terrestrial carbon isotope data (*17*) have also been attributed to a strengthened monsoon circulation due to high pCO_2. However, this technique is not appropriate for regions with precipitation of <600 mm/year or regions that experience a shift in vegetation that involves a change in metabolic pathways (e.g., C4 and CAM plants) or when there is uncertainty in the pCO_2 concentration (*52*), all of which occurs in the EAM region through the Cenozoic. Super-monsoon conditions were established in the Middle to Late Miocene, in agreement with palynological and paleoclimate records, and were caused by intensified easterlies from the South China Sea (Fig. 3), SLLJ and TEJ (figs. S7 and S8) coupled with a strengthened and enlarged Hadley-Walker circulation over EA. The synchronous uplift of the HTR and strengthening EAM is potentially also modified (either dampening or strengthening) by teleconnections arising from paleogeographic changes further afield, for example, changes in the WIS in North America. A focus for future research should be to discern their individual impact on the EAM. Zhang *et al.* (*53*) have suggested that the EAM could be sensitive to the latitudinal position of the HTR due to nonlinear feedbacks on precipitation. If the main body of the elevation stays within ~20°N to ~33°N (as it does generally in our simulations), then it will behave similarly to the Modern. Proxy reconstructions suggest that the most southerly extent of the HTR was at ~16° ± 4°N in the Early Cenozoic. This suggests that HTR latitudinal position may not be a big driver of monsoon evolution during its main uplift phase.

From the mid-Pliocene to the preindustrial there was a reduction in precipitation (Fig. 1), concurrent with a decrease in the height of the IP and a moderate reduction in the height of the Tibetan plateau (<1 km) towards present-day levels (<1 km) towards present-day levels (Fig. 1B), which reduced the northward advection of moisture deeper into the EAM due to a decrease in the coupling strength between the tropics-subtropics.

While this is the first comprehensive combined model-proxy data investigation of the geological history of the EAM system, and the dynamics and mechanisms driving it, there are limitations to the interpretations presented here. Although the model is shown to reproduce the observed monsoon spatial distribution, seasonality, and intensity, the geological-scale response indicated here requires further investigation as well as in other paleoclimate models. This is important to make sure that the dynamical response and mechanisms highlighted are a robust feature and not model dependent. HTR reconstructions are an active arena of ongoing research and will inevitably be further revised. In addition, the decreasing amount of proxy data further back into the geologic record, in particular in the Cretaceous, needs further work so that the trends and implications presented in this study can be fully evaluated with other lines of multiproxy evidence to test the robustness of these results. This is particularly relevant for seasonal proxies in the deep past.

Orbital bias on proxy records and interpretation is also a poorly constrained source of uncertainty (*54*). The location of Northern Hemisphere summer insolation maxima could have an impact on atmospheric circulation and monsoon intensity. If a particular set of proxies from one time slice is biased toward insolation maxima and is compared to a set of proxies in another time slice biased to insolation minima, it could produce strong disparities in the spatiotemporal distribution of precipitation. This would potentially bias the interpretation of change in monsoon intensity and should be a focus for future research.

There are also large uncertainties in the height and extent of HTR topography through time. We have tried to constrain this using reconstructions based on proxy paleoaltimetry data (see the Supplementary Materials for further information). Botsyun *et al.* (*55*) have suggested that the Tibetan Plateau was substantially lower than 3000 m in the Eocene using an isotope-enabled general circulation model (GCM), considerably lower than proxy-based estimates of >4000 m (table S2). Isotope-enabled GCMs have the ability to constrain proxy-based uncertainties and assumptions such as $\delta^{18}O$ moisture source(s), air parcel trajectories, and moisture recycling. However, isotope-enabled GCMs also have an inherent set of uncertainties and assumptions. For example, oceanic and atmospheric circulation will have a large impact on $\delta^{18}O$ source water values and distillation along a trajectory, which is, in part, determined by boundary conditions (e.g., paleogeography, atmospheric composition, ice sheets, and solar luminosity) supplied to the GCM. This makes it difficult to evaluate and compare model-based $\delta^{18}O$ values with proxy-based $\delta^{18}O$ observations. Although we have shown that paleogeography is the dominant driver of the monsoon, the slope of the precipitation trend highlighted in this study is influenced by our current knowledge of the local and regional topography. Hence, additional model simulations could be run following any significant advances in our understanding of Tibetan uplift. Likewise, model resolution is another important consideration. Atmospheric circulation and the precipitation response can be dependent on resolution for certain regions such as the Indian monsoon (*56*). The impact of model resolution on geological-scale monsoon evolution, and whether better-resolved local-scale features fundamentally change the regional-scale climatological response, is uncertain. However, computational cost makes the use of higher-resolution models challenging for simulations of the geologic past. A comparison of different time slices with different model resolutions to constrain this uncertainty should also be a focus of further investigation.

Last, there are uncertainties associated with the model itself. For example, it is known that most climate models of this generation, including HadCM3L, struggle to reproduce proxy estimates of high-latitude warming in greenhouse climates at appropriate CO_2 concentrations (*57*). When equator-to-pole temperature gradients are reduced,

the ITCZ component of a monsoon is likely to weaken (*58*). However, this effect is not as large as might be expected in the EAM region. Hawcroft *et al.* (*59*) show that with a reduction in latitudinal temperature gradient, although there are significant changes in precipitation over oceans, the EAM region is only marginally affected.

MATERIALS AND METHODS

Experimental design

The objectives of this study are twofold: (i) to quantitatively reconstruct the geological-scale onset and evolution of the EAM and (ii) to explore the potential main processes and driving mechanisms that force the observed signal.

Proxy-based reconstruction of monsoon evolution

The proxy data (Fig. 1A) used are a combination of studies from plant flora and fauna (table S1) and other indirect terrestrial and marine proxies used to derive precipitation estimates. An issue with reconstructing monsoon precipitation history in EA is that the monsoon is highly spatially variable, being wetter, warmer, colder, or windier from one location to the next, due to local processes associated with, for example, topographic height and steepness. Hence, individual proxies should not be taken as indicative of a wider regional signal alone. Therefore, we only present data that are made up of a large number of underlying sites, covering a relatively large area. The use of multiproxies can alleviate the problem of low spatial and temporal resolution given enough data sites. Both qualitative (indirect terrestrial and marine proxies, e.g., pollen, climatically sensitive sediments) and quantitative precipitation records derived from nearest living relative (NLR) or climate leaf analysis multivariate program (CLAMP) are used.

The average values (table S1) from the various proxies are binned into their appropriate geologic stage (i.e., Albian stage mid-point, ~105 Ma). Only data that span at least three geologic-stage boundaries are used in the analysis.

The average of the proxy data points are then scaled between 0 and 1 (Eq. 1) to form a normalized precipitation for stage *j*, NP_j

$$NP_j = \frac{\bar{p}_j - 350}{1400 - 350} \quad (1)$$

where the mean precipitation (mm/day) in the EA region for stage *j*, $\bar{p}_j$, is given by

$$\bar{p}_j = \frac{1}{n} \Sigma_{i=0}^{m} P_i \quad (2)$$

where P_i (mm/day) is the precipitation value from site *i*, from a total of *n* sites for stage *j*. The NP for the various stages then forms the trends in Fig. 1A.

Model simulations of monsoon evolution

The reconstruction of tectonics, structures, and depositional environments that underpin this study was created by Getech Plc. The paleodigital elevation models used as boundary conditions (topography, bathymetry, ice sheets) in the model for each stage are informed by these reconstructions, which are, in turn, constrained by extensive geological databases. The paleogeographies were produced at an original resolution of 0.5° × 0.5°, and from these we generated model-resolution (3.75° × 2.5°) land-sea mask, topography and bathymetry, and the subgrid-scale orographic variables required by the model. These model-resolution paleogeographies are shown in fig. S1. For a robust comparison of model precipitation versus the proxy record, we consistently rotate the modern-day monsoon region back through time with the paleogeographies. In addition, we carry out six simulations (stages: Valanginian, Albian, Turonian, Maastrichtian, Chattian, and Piacenzian) with paleogeographies produced independently from, but using similar methods to, the Getech paleogeographies. These are illustrated in fig. S8. The HadCM3L GCM version 4.5 (3.75° × 2.5° longitude × latitude atmosphere and ocean resolution), which is a low-resolution version of HadCM3 (atmosphere resolution, 3.75° × 2.5°; ocean resolution, 1.25° × 1.25°), is used for these model simulations. A comprehensive description and HTR topographic boundary conditions and model skill are provided in the Supplementary Materials. The simulations described in this paper, except for those of the Neogene, and the CO_2 and paleogeography sensitivity studies, are described in detail, including their experimental design, by Lunt *et al.* (*60*). Here follows a brief summary of the key points of the experimental design and model initiation and spin-up. For consistency, all simulations use a modern-day orbital configuration. The paleogeographic sensitivity studies are carried out at various CO_2 concentrations and integrated for varying lengths of time, although all are run for more than 8000 years, and all simulations have reached a steady state in the atmosphere at the surface. To further ascertain the sensitivity of the monsoon system to pCO_2, a series of 15 sensitivity studies were carried out (detailed in Fig. 1C). The pCO_2 sensitivity simulations follow the same methodology as the other simulations. However, in the last 1000 years of the simulation, the pCO_2 concentration was modified (either to 2×, 3×, or 4× preindustrial concentrations) to allow the simulation to approach equilibrium. The prescribed pCO_2 for all the simulations is shown in Fig. 1C. For more detailed Materials and Methods, see the Supplementary Materials.

SUPPLEMENTARY MATERIALS

Supplementary material for this article is available at http://advances.sciencemag.org/cgi/content/full/5/10/eaax1697/DC1

Supplementary Text

Table S1. Proxy precipitation data in the East Asia Monsoon region.

Table S2. Summary and comparison of proxy paleoaltimetry and model paleogeography.

Table S3. GCM sensitivity simulations for each geologic stage-specific simulation June–September (JJAS) data for the strength of the Hadley circulation (vertical velocities; Pa/s) over 21.75°N to 38.75°N and between 1000 and 200 hPa in EA.

Table S4. Correlations between different processes during all geologic stages, Cretaceous stages, Paleogene stages, and Neogene stages.

Fig. S1. Orography and bathymetry.

Fig. S2. EA proxy paleoaltimetry data versus prescribed paleogeography.

Fig. S3. Precipitation seasonality.

Fig. S4. Monsoonal regions.

Fig. S5. Simulation spin-up of SST and zonal 1.5-m air temperature (°C).

Fig. S6. Preindustrial mean fields.

Fig. S7. Wind profiles and vertical velocities in the Hauterivian, Santonian, and Zanclean.

Fig. S8. Mean SLLJ strength and alternative paleogeographies.

References (*61*–*132*)

REFERENCES AND NOTES

1. A. G. Turner, H. Annamalai, Climate change and the South Asian summer monsoon. *Nat. Clim. Chang.* **2**, 587–595 (2012).
2. Z. H. Jiang, J. Song, L. Li, W. Chen, Z. Wang, J. Wang, Extreme climate events in China: IPCC-AR4 model evaluation and projection. *Clim. Chang.* **110**, 385–401 (2012).
3. G. L. Foster, D. L. Royer, D. J. Lunt, Future climate forcing potentially without precedent in the last 420 million years. *Nat. Commun.* **8**, 14845 (2017).

4. Z. T. Guo, B. Sun, Z. S. Zhang, S. Z. Peng, G. Q. Xiao, J. Y. Ge, Q. Z. Hao, Y. S. Qiao, M. Y. Liang, J. F. Liu, Q. Z. Yin, J. J. Wei, A major reorganization of Asian climate by the early Miocene. *Clim. Past* **4**, 153–174 (2008).
5. P. D. Clift, K. V. Hodges, D. Heslop, R. Hannigan, H. Van Long, G. Calves, Correlation of Himalayan exhumation rates and Asian monsoon intensity. *Nat. Geosci.* **1**, 875–880 (2008).
6. X. Sun, P. Wang, How old is the Asian monsoon system?—Palaeobotanical records from China. *Palaeogeogr. Palaeoclimatol. Palaeoecol.* **222**, 181–222 (2005).
7. B. Wang, Q. H. Ding, Global monsoon: Dominant mode of annual variation in the tropics. *Dyn. Atmos. Oceans* **44**, 165–183 (2008).
8. A. Licht, M. van Cappelle, H. A. Abels, J.-B. Ladant, J. Trabucho-Alexandre, C. France-Lanord, Y. Donnadieu, J. Vandenberghe, T. Rigaudier, C. Lécuyer, D. Terry Jr., R. Adriaens, A. Boura, Z. Guo, A. N. Soe, J. Quade, G. Dupont-Nivet, J.-J. Jaeger, Asian monsoons in a late Eocene greenhouse world. *Nature* **513**, 501–506 (2014).
9. R. Spicer, J. Yang, A. Herman, T. Kodrul, G. Aleksandrova, N. Maslova, T. Spicer, L. Ding, Q. Xu, A. Shukla, G. Srivastava, R. Mehrotra, X.-Y. Liu, J.-H. Jin, Paleogene monsoons across India and South China: Drivers of biotic change. *Gondwana Res.* **49**, 350–363 (2017).
10. J. C. Zachos, G. R. Dickens, R. E. Zeebe, An early Cenozoic perspective on greenhouse warming and carbon-cycle dynamics. *Nature* **451**, 279–283 (2008).
11. R. Zhang, D. B. Jiang, Z. S. Zhang, E. T. Yu, The impact of regional uplift of the Tibetan Plateau on the Asian monsoon climate. *Palaeogeogr. Palaeoclimatol. Palaeoecol.* **417**, 137–150 (2015).
12. M. Huber, A. Goldner, Eocene monsoons. *J. Asian Earth Sci.* **44**, 3–23 (2012).
13. J. S. Nie, R. Zhang, C. Necula, D. Heslop, Q. Liu, L. Gong, S. Banerjee, Late Miocene- early Pleistocene paleoclimate history of the Chinese Loess Plateau revealed by remanence unmixing. *Geophys. Res. Lett.* **41**, 2163–2168 (2014).
14. Intergovernmental Panel on Climate Change, *Climate Change 2013: The Physical Science Basis. Contribution of Working Group I to the Fifth Assessment Report of the Intergovernmental Panel on Climate Change* (Cambridge Univ. Press, 2013), p. 1535.
15. M. Pagani, J. C. Zachos, K. H. Freeman, B. Tipple, S. Bohaty, Marked decline in atmospheric carbon dioxide concentrations during the Paleogene. *Science* **309**, 600–603 (2005).
16. J. M. Chen, P. Zhao, C. S. Wang, Y. J. Huang, K. Cao, Modeling East Asian climate and impacts of atmospheric CO_2 concentration during the Late Cretaceous (66 Ma). *Palaeogeogr. Palaeoclimatol. Palaeoecol.* **385**, 190–201 (2013).
17. J. K. C. Rugenstein, C. P. Chamberlain, The evolution of hydroclimate in Asia over the Cenozoic: A stable-isotope perspective. *Earth Sci. Rev.* **185**, 1129–1156 (2018).
18. F. Hourdin, I. Musat, F. se Guichard, P. M. Ruti, F. Favot, M.-A. Filiberti, M. Pham, J.-Y. Grandpeix, J. Polcher, P. Marquet, A. Boone, J.-P. Lafore, J.-L. Redelsperger, A. Dell'aquila, T. L. Doval, A. K. Traore, H. Gallée, AMMA-Model Intercomparison Project. *Bull. Am. Meteorol. Soc.* **91**, 95–104 (2010).
19. A. Cherchi, A. Alessandri, S. Masina, A. Navarra, Effects of increased CO_2 levels on monsoons. *Clim. Dyn.* **37**, 83–101 (2011).
20. W. R. Boos, T. Storelvmo, Near-linear response of mean monsoon strength to a broad range of radiative forcings. *Proc. Natl. Acad. Sci. U.S.A.* **113**, 1510–1515 (2016).
21. G. Roe, Q. Ding, D. S. Battisti, P. Molnar, M. K. Clark, C. N. Garzione, A modeling study of the response of Asian summertime climate to the largest geologic forcings of the past 50 Ma. *J. Geophys. Res.-Atmos.* **121**, 5453–5470 (2016).
22. P. J. Valdes, B. W. Sellwood, G. D. Price, Evaluating concepts of Cretaceous equability. Palaeoclimates. *Data Model.* **2**, 139–158 (1996).
23. E. J. Barron, L. A. Frakes, in *Phosphates of the World, Neogene to Modern phosphorites*, W. C. Burnett, S. R. Riggs, Eds. (Cambridge Univ. Press, International Geological Correlation Programme Project 156: Phosphorites, 1990), vol. 3, pp. 261–272.
24. G. D. Hoke, J. Liu-Zeng, M. T. Hren, G. K. Wissink, C. N. Garzione, Stable isotopes reveal high southeast Tibetan Plateau margin since the Paleogene. *Earth Planet. Sci. Lett.* **394**, 270–278 (2014).
25. J. Quade, D. O. Breecker, M. Daeron, J. Eiler, The paleoaltimetry of Tibet: An isotopic perspective. *Am. J. Sci.* **311**, 77–115 (2011).
26. C. Wang, J. Dai, X. Zhao, Y. Li, S. A. Graham, D. He, B. Ran, J. Meng, Outward-growth of the Tibetan Plateau during the Cenozoic: A review. *Tectonophysics* **621**, 1–43 (2014).
27. P. Bouilhol, O. Jagoutz, J. M. Hanchar, F. O. Dudas, Dating the India-Eurasia collision through arc magmatic records. *Earth Planet. Sci. Lett.* **366**, 163–175 (2013).
28. G. Ramstein, F. Fluteau, J. Besse, S. Joussaume, Effect of orogeny, plate motion and land sea distribution on Eurasian climate change over the past 30 million years. *Nature* **386**, 788–795 (1997).
29. G. X. Wu, Y. Liu, B. Dong, X. Liang, A. Duan, Q. Bao, J. Yu, Revisiting Asian monsoon formation and change associated with Tibetan Plateau forcing: I. Formation. *Clim. Dyn.* **39**, 1169–1181 (2012).
30. E. Anagnostou, E. H. John, K. M. Edgar, G. L. Foster, A. Ridgwell, G. N. Inglis, R. D. Pancost, D. J. Lunt, P. N. Pearson, Changing atmospheric CO2 concentration was the primary driver of early Cenozoic climate. *Nature* **533**, 380–384 (2016).
31. H. Hasegawa, R. Tada, X. Jiang, Y. Suganuma, S. Imsamut, P. Charusiri, N. Ichinnorov, Y. Khand, Drastic shrinking of the Hadley circulation during the mid-Cretaceous Supergreenhouse. *Clim. Past* **8**, 1323–1337 (2012).
32. P. D. Clift, S. Wan, J. Blusztajn, Reconstructing chemical weathering, physical erosion and monsoon intensity since 25 Ma in the northern South China Sea: A review of competing proxies. *Earth Sci. Rev.* **130**, 86–102 (2014).
33. P. X. Wang, B. Wang, H. Cheng, J. Fasullo, Z. T. Guo, T. Kiefer, Z. Y. Liu, The global monsoon across timescales: Coherent variability of regional monsoons. *Clim. Past* **10**, 2007–2052 (2014).
34. Q. Wang, R. A. Spicer, J. Yang, Y.-F. Wang, C.-S. Li, The Eocene climate of China, the early elevation of the Tibetan Plateau and the onset of the Asian Monsoon. *Glob. Chang. Biol.* **19**, 3709–3728 (2013).
35. C. Quan, Y.-S. Liu, T. Utescher, Paleogene temperature gradient, seasonal variation and climate evolution of northeast China. *Palaeogeogr. Palaeoclimatol. Palaeoecol.* **313–314**, 150–161 (2012).
36. C. Quan, Y.-S. Liu, T. Utescher, Eocene monsoon prevalence over China: A paleobotanical perspective. *Palaeogeogr. Palaeoclimatol. Palaeoecol.* **365–366**, 302–311 (2012).
37. J. Dabang, W. Huijun, L. Xianmei, Evaluation of East Asian climatology as simulated by seven coupled models. *Adv. Atmos. Sci.* **22**, 479–495 (2005).
38. K. Sperber, H. Annamalai, I.-S. Kang, A. Kitoh, A. Moise, A. Turner, B. Wang, T. Zhou, The Asian summer monsoon: An intercomparison of CMIP5 vs. CMIP3 simulations of the late 20th century. *Clim. Dyn.* **41**, 2711–2744 (2013).
39. P. Xie, P. A. Arkin, Global precipitation: A 17-year monthly analysis based on gauge observations, satellite estimates, and numerical model outputs. *Bull. Am. Meteorol. Soc.* **78**, 2539–2558 (1997).
40. E. A. Jarzembowski, R. A. Spicer, D. Cantrill, Cretaceous Phytogeography and Climate Signals - Discussion. *Philos. Trans. R. Soc. Lond. B* **341**, 285–286 (1993).
41. A. Zarrin, H. Ghaemi, M. Azadi, A. Mofidi, E. Mirzaei, The effect of the Zagros Mountains on the formation and maintenance of the Iran Anticyclone using $RegCM_4$. *Meteorog. Atmos. Phys.* **112**, 91–100 (2011).
42. A. Licht, G. Dupont-Nivet, A. Pullen, P. Kapp, H. A. Abels, Z. Lai, Z. Guo, J. Abell, D. Giesler, Resilience of the Asian atmospheric circulation shown by Paleogene dust provenance. *Nat. Commun.* **7**, 12390 (2016).
43. R. A. Spicer, J. Yang, A. B. Herman, T. Kodrul, N. Maslova, T. E. V. Spicer, G. Aleksandrova, J. Jin, Asian Eocene monsoons as revealed by leaf architectural signatures. *Earth Planet. Sci. Lett.* **449**, 61–68 (2016).
44. A. A. G. Webb, H. Guo, P. D. Clift, L. Husson, T. Müller, D. Costantino, A. Yin, Z. Xu, H. Cao, Q. Wang, The Himalaya in 3D: Slab dynamics controlled mountain building and monsoon intensification. *Lithosphere* **9**, 637–651 (2017).
45. B. Hoskins, B. Wang, in *The Asian Monsoon*, B. Wang, Ed. (Praxis Publishing Ltd., Chichester, 2006), p. 787.
46. X. S. Jiang, Z. Pan, J. Xu, X. Li, G. Xie, Z. Xiao, Late Cretaceous aeolian dunes and reconstruction of palaeo-wind belts of the Xinjiang Basin, Jiangxi Province, China. *Palaeogeogr. Palaeoclimatol. Palaeoecol.* **257**, 58–66 (2008).
47. H. Weng, K. Ashok, S. Behera, S. Rao, T. Yamagata, Impacts of recent El Nino Modoki on dry/wet conditions in the Pacific rim during boreal summer. *Clim. Dyn.* **29**, 113–129 (2007).
48. M. J. Rodwell, B. J. Hoskins, Subtropical anticyclones and summer monsoons. *J. Clim.* **14**, 3192–3211 (2001).
49. W. Yanase, A. Abe-Ouchi, The LGM surface climate and atmospheric circulation over East Asia and the North Pacific in the PMIP2 coupled model simulations. *Clim. Past* **3**, 439–451 (2007).
50. L. Li, Y. C. Zhang, Effects of Different Configurations of the East Asian Subtropical and Polar Front Jets on Precipitation during the Mei-Yu Season. *J. Clim.* **27**, 6660–6672 (2014).
51. Y. Zhao, M. Wang, A. Huang, H. Li, W. Huo, Q. Yang, Relationships between the West Asian subtropical westerly jet and summer precipitation in northern Xinjiang. *Theor. Appl. Climatol.* **116**, 403–411 (2014).
52. A. Takeuchi, M. Hren, S. V. Smith, C. P. Chamberlain, P. B. Larson, Pedogenic carbonate carbon isotopic constraints on paleoprecipitation: Evolution of desert in the Pacific Northwest, USA, in response to topographic development of the Cascade Range. *Chem. Geol.* **277**, 323–335 (2010).
53. R. Zhang, D. Jiang, G. Ramstein, Z. Zhang, P. C. Lippert, E. Yu, Changes in Tibetan Plateau latitude as an important factor for understanding East Asian climate since the Eocene: A modeling study. *Earth Planet. Sci. Lett.* **484**, 295–308 (2018).
54. C. R. Tabor, B. L. Otto-Bliesner, E. C. Brady, J. Nusbaumer, J. Zhu, M. P. Erb, T. E. Wong, Z. Liu, D. Noone, Interpreting Precession-Driven $\delta^{18}O$ Variability in the South Asian Monsoon Region. *J. Geophys. Res. Atmos.* **123**, 5927–5946 (2018).
55. S. Botsyun, P. Sepulchre, Y. Donnadieu, C. Risi, A. Licht, J. K. C. Rugenstein, Revised paleoaltimetry data show low Tibetan Plateau elevation during the Eocene. *Science* **363**, eaaq1436 (2019).

56. R. P. Acosta, M. Huber, The neglected Indo-Gangetic Plains low-level jet and its importance for moisture transport and precipitation during the peak summer monsoon. *Geophys. Res. Lett.* **44**, 8601–8610 (2017).
57. D. J. Lunt, T. D. Jones, M. Heinemann, M. Huber, A. LeGrande, A. Winguth, C. Loptson, J. Marotzke, C. D. Roberts, J. Tindall, P. Valdes, C. Winguth, A model-data comparison for a multi-model ensemble of early Eocene atmosphere-ocean simulations: EoMIP. *Clim. Past* **8**, 1717–1736 (2012).
58. Y. Sun, G. Ramstein, C. Contoux, T. Zhou, A comparative study of large-scale atmospheric circulation in the context of a future scenario (RCP4.5) and past warmth (mid-Pliocene). *Clim. Past* **9**, 1613–1627 (2013).
59. M. Hawcroft, J. M. Haywood, M. Collins, A. Jones, The contrasting climate response to tropical and extratropical energy perturbations. *Clim. Dyn.* **51**, 3231–3249 (2018).
60. D. J. Lunt, A. Farnsworth, C. Loptson, G. L. Foster, P. Markwick, C. L. O'Brien, R. D. Pancost, S. A. Robinson, N. Wrobel, Palaeogeographic controls on climate and proxy interpretation. *Clim. Past* **12**, 1181–1198 (2016).
61. J. A. Wolfe, Palaeobotanical evidence for a marked temperature increase following the Cretaceous tertiary boundary. *Nature* **343**, 153–156 (1990).
62. Y. Horiuchi, P. Charusiri, K.-i. Hisada, Identification of an anastomosing river system in the Early Cretaceous Khorat Basin, northeastern Thailand, using stratigraphy and paleosols. *J. Asian Earth Sci.* **61**, 62–77 (2012).
63. P. J. Markwick, P. J. Valdes, Palaeo-digital elevation models for use as boundary conditions in coupled ocean-atmo sphere GCM experiments: A Maastrichtian (late Cretaceous) example. *Palaeogeogr. Palaeoclimatol. Palaeoecol.* **213**, 37–63 (2004).
64. A. Ziegler, M., D. B. Rowley, in *Tectonic Boundary Conditions for Climate Reconstructions*, T. J. Crowley, K. C. Burke, Eds. (Oxford Monographs on Geology and Geophysics Oxford, 1998), vol. 39, pp. 147–165.
65. R. Spicer, S. Bera, S. De Bera, T. E. V. Spicer, G. Srivastava, R. Mehrotra, N. Mehrotra, J. Yang, Why do foliar physiognomic climate estimates sometimes differ from those observed? Insights from taphonomic information loss and a CLAMP case study from the Ganges Delta. *Palaeogeogr. Palaeoclimatol. Palaeoecol.* **302**, 381–395 (2011).
66. A. Farnsworth, E. White, C. J. R. Williams, E. Black, D. R. Kniveton, in *African Climate and Climate Change: Physical, Social and Political Perspectives,* C. J. R. Williams, D. R. Kniveton, Eds. (Springer Netherlands, 2011), pp. 101–122.
67. M. New, M. Hulme, P. Jones, Representing twentieth-century space-time climate variability. Part I: Development of a 1961-90 mean monthly terrestrial climatology. *J. Clim.* **12**, 829–856 (1999).
68. P. Markwick, in *Deep-Time Perspectives on Climate Change: Marrying the Signal from Computer Models and Biological Proxies*, M. Willams, A. Haywood, F. Gregory, D. Schmidt, Eds. (The Micropaleontological Society Special Publications, 2007), pp. 251–312.
69. C. Gordon, C. Cooper, C. A. Senior, H. Banks, J. M. Gregory, T. C. Johns, J. F. B. Mitchell, R. A. Wood, The simulation of SST, sea ice extents and ocean heat transports in a version of the Hadley Centre coupled model without flux adjustments. *Clim. Dyn.* **16**, 147–168 (2000).
70. M. Collins, S. F. B. Tett, C. Cooper, The internal climate variability of HadCM3, a version of the Hadley Centre coupled model without flux adjustments. *Clim. Dyn.* **17**, 61–81 (2001).
71. J. M. Edwards, A. Slingo, Studies with a flexible new radiation code .1. Choosing a configuration for a large-scale model. *Q. J. R. Meteorol. Soc.* **122**, 689–719 (1996).
72. J. M. Gregory, J. F. B. Mitchell, The climate response to CO_2 of the Hadley Centre coupled AOGCM with and without flux adjustment. *Geophys. Res. Lett.* **24**, 1943–1946 (1997).
73. Met. Office, *Description of the "TRIFFID" Dynamic Global Vegetation Model* (2001).
74. P. R. Gent, J. C. Mcwilliams, Isopycnal mixing in ocean circulation models. *J. Phys. Oceanogr.* **20**, 150–155 (1990).
75. W. D. Hibler III, Dynamic thermodynamic sea ice model. *J. Phys. Oceanogr.* **9**, 815–846 (1979).
76. H. Cattle, J. Crossley, D. J. Drewry, Modeling arctic climate-change. *Philos. Trans. R. Soc. A* **352**, 201–213 (1995).
77. C. A. Loptson, D. J. Lunt, J. E. Francis, Investigating vegetation-climate feedbacks during the early Eocene. *Clim. Past* **10**, 419–436 (2014).
78. K. Takata, K. Saito, T. Yasunari, Changes in the Asian monsoon climate during 1700-1850 induced by preindustrial cultivation. *Proc. Natl. Acad. Sci. U.S.A.* **106**, 9586–9589 (2009).
79. P. J. Valdes, E. Armstrong, M. P. S. Badger, C. D. Bradshaw, F. Bragg, M. Crucifix, T. Davies-Barnard, J. J. Day, A. Farnsworth, C. Gordon, P. O. Hopcroft, A. T. Kennedy, N. S. Lord, D. J. Lunt, A. Marzocchi, L. M. Parry, V. Pope, W. H. G. Roberts, E. J. Stone, G. J. L. Tourte, J. H. T. Williams, The BRIDGE HadCM3 family of climate models: HadCM3@Bristol v1.0. *Geosci. Model Dev. Discuss.* **10**, 3715–3743 (2017).
80. U. Schneider, A. Becker, P. Finger, A. Meyer-Christoffer, M. Ziese, B. Rudolf, GPCC's new land surface precipitation climatology based on quality-controlled in situ data and its role in quantifying the global water cycle. *Theor. Appl. Climatol.* **115**, 15–40 (2014).
81. Y. Li, R. Lu, B. Dong, The ENSO-Asian monsoon interaction in a coupled ocean-atmosphere GCM. *J. Clim.* **20**, 5164–5177 (2007).
82. E. Gasson, D. J. Lunt, R. DeConto, A. Goldner, M. Heinemann, M. Huber, A. N. LeGrande, D. Pollard, N. Sagoo, M. Siddall, A. Winguth, P. J. Valdes, Uncertainties in the modelled CO2 threshold for Antarctic glaciation. *Clim. Past* **10**, 451–466 (2014).
83. D. O. Gough, Solar interior structure and luminosity variations. *Sol. Phys.* **74**, 21–34 (1981).
84. D. Luthi, M. L. Floch, B. Bereiter, T. Blunier, J.-M. Barnola, U. Siegenthaler, D. Raynaud, J. Jouzel, H. Fischer, K. Kawamura, T. F. Stocker, High-resolution carbon dioxide concentration record 650,000-800,000 years before present. *Nature* **453**, 379–382 (2008).
85. P. A. Arkin, P. P. Xie, The Climate Data Guide: CMAP: CPC Merged Analysis of Precipitation (2014); https://climatedataguide.ucar.edu/climate-data/cmap-cpc-merged-analysis-precipitation#sthash.zampwaxF.dpuf.
86. A. Zhisheng, J. E. Kutzbach, W. L. Prell, S. C. Porter, Evolution of Asian monsoons and phased uplift of the Himalayan Tibetan plateau since Late Miocene times. *Nature* **411**, 62–66 (2001).
87. Y. Xie, F. Wu, X. Fang, Middle Eocene East Asian monsoon prevalence over southern China: Evidence from palynological records. *Glob. Planet. Chang.* **175**, 13–26 (2019).
88. L.-C. Zhao, Y.-F. Wang, C.-J. Liu, C.-S. Li, Climatic implications of fruit and seed assemblage from Miocene of Yunnan, southwestern China. *Quat. Int.* **117**, 81–89 (2004).
89. J. Yang, Y.-F. Wang, R. A. Spicer, V. Mosbrugger, C.-S. Li, Q.-G. Sun, Climatic reconstruction at the miocene shanwang basin, China, using leaf margin analysis, clamp, coexistence approach, and overlapping distribution analysis. *Am. J. Bot.* **94**, 599–608 (2007).
90. J.-X. Xu, D. K. Ferguson, C.-S. Li, Y.-F. Wang, Late Miocene vegetation and climate of the Luhe region in Yunnan, southwestern China. *Rev. Palaeobot. Palynol.* **148**, 36–59 (2008).
91. Y. W. Xing, T. Utescher, F. M. B. Jacques, T. Su, Y. Liu, Y. Huang, Z. Zhou, Paleoclimatic estimation reveals a weak winter monsoon in southwestern China during the late Miocene: Evidence from plant macrofossils. *Palaeogeogr. Palaeoclimatol. Palaeoecol.* **358**, 19–26 (2012).
92. F. M. B. Jacques, S.-X. Guo, T. Su, Y.-W. Xing, Y.-J. Huang, Y.-S. Liu, D. K. Ferguson, Z.-K. Zhou, Quantitative reconstruction of the Late Miocene monsoon climates of southwest China: A case study of the Lincang flora from Yunnan Province. *Palaeogeogr. Palaeoclimatol. Palaeoecol.* **304**, 318–327 (2011).
93. T. Su, F. M. B. Jacques, R. A. Spicer, Y.-S. Liu, Y.-J. Huang, Y.-W. Xing, Z.-K. Zhou, Post-Pliocene establishment of the present monsoonal climate in SW China: Evidence from the late Pliocene Longmen megaflora. *Clim. Past* **9**, 1911–1920 (2013).
94. S. P. Xie, B. Sun, J. Wu, Z. Lin, D. Yan, L. Xiao, Palaeodimatic estimates for the late Pliocene based on leaf physiognomy from western Yunnan, China. *Turk. J. Earth Sci.* **21**, 251–261 (2012).
95. K. Xia, T. Su, Y.-S. Liu, Y.-W. Xing, F. M. B. Jacques, Z.-K. Zhou, Quantitative climate reconstructions of the late Miocene Xiaolongtan megaflora from Yunnan, southwest China. *Palaeogeogr. Palaeoclimatol. Palaeoecol.* **276**, 80–86 (2009).
96. Y.-F. Yao, A. A. Bruch, V. Mosbrugger, C.-S. Li, Quantitative reconstruction of Miocene climate patterns and evolution in Southern China based on plant fossils. *Palaeogeogr. Palaeoclimatol. Palaeoecol.* **304**, 291–307 (2011).
97. Q.-g. Sun, M. E. Collinson, C.-S. Li, Y.-F. Wang, D. J. Beerling, Quantitative reconstruction of palaeoclimate from the Middle Miocene Shanwang flora, eastern China. *Palaeogeogr. Palaeoclimatol. Palaeoecol.* **180**, 315–329 (2002).
98. B.-N. Sun, J.-Y. Wu, Y.-S. Liu, S.-T. Ding, X.-C. Li, S.-P. Xie, D.-F. Yan, Z.-C. Lin, Reconstructing Neogene vegetation and climates to infer tectonic uplift in western Yunnan, China. *Palaeogeogr. Palaeoclimatol. Palaeoecol.* **304**, 328–336 (2011).
99. Y.-F. Yao, S. Bera, D. K. Ferguson, V. Mosbrugger, K. N. Paudayal, J.-H. Jin, C.-S. Li, Reconstruction of paleovegetation and paleoclimate in the Early and Middle Eocene, Hainan Island, China. *Clim. Chang.* **92**, 169–189 (2009).
100. Y. S. Liu, T. Utescher, Z. K. Zhou, B. N. Sun, The evolution of Miocene climates in North China: Preliminary results of quantitative reconstructions from plant fossil records. *Palaeogeogr. Palaeoclimatol. Palaeoecol.* **304**, 308–317 (2011).
101. X.-Y. Kou, D. K. Ferguson, J.-X. Xu, Y.-F. Wang, C.-S. Li, The reconstruction of paleovegetation and paleoclimate in the Late Pliocene of West Yunnan, China. *Clim. Chang.* **77**, 431–448 (2006).
102. H. Hao, D. K. Ferguson, H. Chang, C.-S. Li, Vegetation and climate of the Lop Nur area, China, during the past 7 million years. *Clim. Chang.* **113**, 323–338 (2012).
103. C. Quan, Y.-S. Liu, T. Utescher, Paleogene evolution of precipitation in northeastern China supporting the middle Eocene intensification of the East Asian monsoon. *Palaios* **26**, 743–753 (2011).
104. Y. Wang, T. Deng, D. Biasatti, Ancient diets indicate significant uplift of southern Tibet after ca. 7 Ma. *Geology* **34**, 309–312 (2006).
105. Q. Xu, L. Ding, L. Zhang, D. Yang, F. Cai, Q. Lai, J. Liu, R. Shi, Stable isotopes of modern herbivore tooth enamel in the Tibetan Plateau: Implications for paleoelevation reconstructions. *Chin. Sci. Bull.* **55**, 45–54 (2010).

106. D. B. Rowley, R. T. Pierrehumbert, B. S. Currie, A new approach to stable isotope-based paleoaltimetry: Implications for paleoaltimetry and paleohypsometry of the High Himalaya since the Late Miocene. *Earth Planet. Sci. Lett.* **188**, 253–268 (2001).
107. C. N. Garzione, D. L. Dettman, J. Quade, P. G. DeCelles, R. F. Butler, High times on the Tibetan Plateau: Paleoelevation of the Thakkhola graben, Nepal. *Geology* **28**, 339–342 (2000).
108. K. W. Huntington, J. Saylor, J. Quade, A. M. Hudson, High late Miocene-Pliocene elevation of the Zhada Basin, southwestern Tibetan Plateau, from carbonate clumped isotope thermometry. *Geol. Soc. Am. Bull.* **127**, 181–199 (2015).
109. J. E. Saylor, J. Quade, D. L. Dettman, P. G. DeCelles, P. A. Kapp, L. Ding, The late Miocene through present paleoelevation history of southwestern Tibet. *Am. J. Sci.* **309**, 1–42 (2009).
110. M. A. Murphy, J. E. Saylor, L. Ding, Late Miocene topographic inversion in southwest Tibet based on integrated paleoelevation reconstructions and structural history. *Earth Planet. Sci. Lett.* **282**, 1–9 (2009).
111. A. Gebelin, A. Mulch, C. Teyssier, M. J. Jessup, R. D. Law, M. Brunel, The Miocene elevation of Mount Everest. *Geology* **41**, 799–802 (2013).
112. L. Ding, R. A. Spicer, J. Yang, Q. Xu, F. Cai, S. Li, Q. Lai, H. Wang, T. E. V. Spicer, Y. Yue, A. Shukla, G. Srivastava, M. A. Khan, S. Bera, R. Mehrotra, Quantifying the rise of the Himalaya orogen and implications for the South Asian monsoon. *Geology* **45**, 215–218 (2017).
113. B. S. Currie, P. J. Polissar, D. B. Rowley, M. Ingalls, S. Li, G. Olack, K. H. Freeman, Multiproxy paleoaltimetry of the late Oligocene-Pliocene Oiyug basin, southern Tibet. *Am. J. Sci.* **316**, 401–436 (2016).
114. B. S. Currie, D. B. Rowley, N. J. Tabor, Middle Miocene paleoaltimetry of southern Tibet: Implications for the role of mantle thickening and delamination in the Himalayan orogen. *Geology* **33**, 181–184 (2005).
115. R. A. Spicer, N. B. W. Harris, M. Widdowson, A. B. Herman, S. Guo, P. J. Valdes, J. A. Wolfe, S. P. Kelley, Constant elevation of southern Tibet over the past 15 million years. *Nature* **421**, 622–624 (2003).
116. M. A. Khan, R. A. Spicer, S. Bera, R. Ghosh, J. Yang, T. E. V. Spicer, S.-x. Guo, T. Su, F. Jacques, P. J. Grote, Miocene to Pleistocene floras and climate of the Eastern Himalayan Siwaliks, and new palaeoelevation estimates for the Namling-Oiyug Basin, Tibet. *Glob. Planet. Chang.* **113**, 1–10 (2014).
117. P. G. DeCelles, P. Kapp, J. Quade, G. E. Gehrels, Oligocene-Miocene Kailas basin, southwestern Tibet: Record of postcollisional upper-plate extension in the Indus-Yarlung suture zone. *Geol. Soc. Am. Bull.* **123**, 1337–1362 (2011).
118. L. Ding, Q. Xu, Y. Yue, H. Wang, F. Cai, S. Li, The Andean-type Gangdese Mountains: Paleoelevation record from the Paleocene-Eocene Linzhou Basin. *Earth Planet. Sci. Lett.* **392**, 250–264 (2014).
119. P. G. DeCelles, P. Kapp, L. Ding, G. E. Gehrels, Late Cretaceous to middle Tertiary basin evolution in the central Tibetan Plateau: Changing environments in response to tectonic partitioning, aridification, and regional elevation gain. *Geol. Soc. Am. Bull.* **119**, 654–680 (2007).
120. D. B. Rowley, B. S. Currie, Palaeo-altimetry of the late Eocene to Miocene Lunpola basin, central Tibet. *Nature* **439**, 677–681 (2006).
121. P. J. Polissar, K. H. Freeman, D. B. Rowley, F. A. McInerney, B. S. Currie, Paleoaltimetry of the Tibetan Plateau from *D/H* ratios of lipid biomarkers. *Earth Planet. Sci. Lett.* **287**, 64–76 (2009).
122. T. Deng, S. Wang, G. Xie, Q. Li, S. Hou, B. Sun, A mammalian fossil from the Dingqing Formation in the Lunpola Basin, northern Tibet, and its relevance to age and paleo-altimetry. *Chin. Sci. Bull.* **57**, 261–269 (2012).
123. J. M. Sun, Q. Xu, W. Liu, Z. Zhang, L. Xue, P. Zhao, Palynological evidence for the latest Oligocene-early Miocene paleoelevation estimate in the Lunpola Basin, central Tibet. *Palaeogeogr. Palaeoclimatol. Palaeoecol.* **399**, 21–30 (2014).
124. G. Jia, Y. Bai, Y. Ma, J. Sun, P. Peng, Paleoelevation of Tibetan Lunpola basin in the Oligocene-Miocene transition estimated from leaf wax lipid dual isotopes. *Glob. Planet. Chang.* **126**, 14–22 (2015).
125. Q. Xu, L. Ding, R. Hetzel, Y. Yue, E. Rades, Low elevation of the northern Lhasa terrane in the Eocene: Implications for relief development in south Tibet. *Terra Nova* **27**, 458–466 (2015).
126. R. Hetzel, I. Dunkl, V. Haider, M. Strobl, H. von Eynatten, L. Ding, D. Frei, Peneplain formation in southern Tibet predates the India-Asia collision and plateau uplift. *Geology* **39**, 983–986 (2011).
127. Q. Xu, L. Ding, L. Zhang, F. Cai, Q. Lai, D. Yang, J. Liu-Zeng, Paleogene high elevations in the Qiangtang Terrane, central Tibetan Plateau. *Earth Planet. Sci. Lett.* **362**, 31–42 (2013).
128. S. Li, B. S. Currie, D. B. Rowley, M. Ingalls, Cenozoic paleoaltimetry of the SE margin of the Tibetan Plateau: Constraints on the tectonic evolution of the region. *Earth Planet. Sci. Lett.* **432**, 415–424 (2015).
129. A. J. Cyr, B. S. Currie, D. B. Rowley, Geochemical evaluation of Fenghuoshan Group lacustrine carbonates, North-Central Tibet: Implications for the paleoaltimetry of the Eocene Tibetan Plateau. *J. Geol.* **113**, 517–533 (2005).
130. Y. Miao, F. Wu, H. Chang, X. Fang, T. Deng, J. Sun, C. Jin, A Late-Eocene palynological record from the Hoh Xil Basin, northern Tibetan Plateau, and its implications for stratigraphic age, paleoclimate and paleoelevation. *Gondwana Res.* **31**, 241–252 (2016).
131. J. Sun, B. Alloway, X. Fang, B. F. Windley, Refuting the evidence for an earlier birth of the Taklimakan Desert. *Proc. Natl. Acad. Sci. U.S.A.* **112**, E5556–E5557 (2015).
132. L. Zhang, C. Wang, K. Cao, Q. Wang, J. Tan, Y. Gao, High elevation of Jiaolai Basin during the Late Cretaceous: Implication for the coastal mountains along the East Asian margin. *Earth Planet. Sci. Lett.* **456**, 112–123 (2016).

Acknowledgments: We thank S. Powell for assistance with drafting Fig. 4. **Funding:** A.F., D.J.L., and R.D.P. acknowledge funding from NERC through NE/K014757/1, NE/I005722/1, NE/I005714/1, and (P.J.V. also) NE/P013805/1. S.A.R. acknowledges funding from NERC through NE/K012479/1. D.J.L., R.D.P., and P.J.V. acknowledge funding through ERC grant "The greenhouse earth system" (T-GRES, project reference 340923). **Author contributions:** A.F. and D.J.L. carried out the simulations and wrote the first draft of the paper. S.A.R., P.D.C., and T.S. provided interpretation of the proxy data. P.J.V. and W.H.G.R. provided input on the dynamical interpretation. N.W. provided the required plate tectonic rotations. F.B. provided one simulation. Getech provided the paleogeographies, which were created by the globe team, represented here by S.-J.K. All authors contributed to writing the paper. **Competing interests:** The authors declare that they have no competing interests. **Data and materials availability:** All data needed to evaluate the conclusions in the paper are present in the paper and/or the Supplementary Materials. Model data can be accessed at www.bridge.bris.ac.uk/resources/simulations. Data reported in this paper are also tabulated in tables S1 to S3. Additional data related to this paper may be requested from the authors.

Submitted 27 February 2019
Accepted 17 September 2019
Published 30 October 2019
10.1126/sciadv.aax1697

Citation: A. Farnsworth, D. J. Lunt, S. A. Robinson, P. J. Valdes, W. H. G. Roberts, P. D. Clift, P. Markwick, T. Su, N. Wrobel, F. Bragg, S.-J. Kelland, R. D. Pancost, Past East Asian monsoon evolution controlled by paleogeography, not CO_2. *Sci. Adv.* **5**, eaax1697 (2019).